APCC
APEC CLIMATE CENTER

TECHNICAL REPORT

APCC
APEC CLIMATE CENTER

PREFACE

It is our pleasure to present to you the APEC Climate Center (APCC)'s Technical Report 2011, which reports the core outcomes of our research activities from the past year.

Since 2005, APCC, as a hub of climate information in the Asia-Pacific region, has strived to share our analysis and prediction of abnormal climate and to apply this information to regional development. The center has established the largest Multi-Model Ensemble (MME) system for seasonal prediction through its international science network and has provided value-added products to various stakeholders. Recently, APCC has expanded its mandate to include enhancement of the capacity of APEC member economies information to respond effectively to climate change and variability through better application of climate.

To achieve its research and social objectives, in 2011, APCC made efforts to research improvements in its climate prediction performance from various angles and towards better understanding of climate variability and the reproducibility of the climate models for the relevant application of climate information to society. The following technical report provides more information about our research outcomes from 2011.

APCC will continue to improve the quality and accuracy of climate information, recognizing that the utility of this information is only as good as its quality. We would like to make the best use of our research results for the benefit of society and academia. We also welcome any feedback on this report or on our services.

My best and warmest regards to all of you.

Dr. Chin-Seung Chung
Director/APEC Climate Center

CONTENTS

Improvement of MME Seasonal Prediction Skill Using A Climate Filter Concept

Doo-Young Lee

APCC

TECHNICAL REPORT 2011-02

Improvement of MME Seasonal Prediction Skill Using A Climate Filter Concept

Doo-Young Lee

ABSTRACT

We propose a novel climate 'filter' approach that employs relative dynamical diagnostic performance to enhance the APCC operational multi-model ensemble (MME) hindcasts of precipitation and temperature at 850 hPa over the East Asian summer monsoon region for the boreal summers of 1981-2003. We also evaluate the performance of individual constituent models and compare the results of corresponding observed and reanalyzed data. The filter is based on the strong relationship between the observed and model-simulated ENSO (NAO)-associated EASM indices. The reproducibility of this relationship is utilized to evaluate model performance. It is found the retrospective forecast skill of a newer type of MME that contains only the 'more skillful' models is superior to that of the all-inclusive operational MME. We found that the gap between the skills of MMEs comprising only the more skillful models and those with only the less skillful models significantly widens over the East Asian summer monsoon region. Based on an experimental forecast for two boreal summer seasons, the filtered MME is shown to generally outperform the all inclusive MME, and the proposed method is confirmed to be potentially useful for real time seasonal prediction.

1. Introduction

Many researches indicate that the multi-model ensemble (MME) approach to dynamical climate prediction is effective in reducing the uncertainty arising from atmospheric or oceanic model dynamics and from physical parameterizations of unresolved sub-grid scale processes [Krishnamurti et al., 1999, 2000; Palmer et al., 2000; Shukla et al., 2000; Barnston et al., 2003, Hagedorn et al., 2005; Doblas-Reyes et al., 2000]. The MME approach is known to be a useful and practical way to alleviate the inherent and systematic errors of individual models, as well as to offer better forecast predictability and accuracy through the isolation of observed outcomes from multiple models. Indeed, several studies [Krishnamurti et al., 2000; Palmer et al., 2000; Pavan and Doblas-Reyes, 2000; Peng et al., 2002; Shukla et al., 2000; Hagedorn et al., 2005; Doblas-Reyes et al., 2005; Yun et al., 2005; Min et al., 2009; Wang et al., 2009a] have reported that the performance skill of the MME is typically higher than the skills of the constituent individual models. Encouraged by such results, a number of meteorological centers worldwide now operationally implement dynamical seasonal prediction, often with individual models selected through some in-house

quality control for the identification of problems, such as spurious or missing values [Alves et al., 2003; Palmer et al., 2004; Saha et al., 2006; Lee et al., 2009].

However, operational experience has shown that the prediction skill of the MME approach to be relatively limited for some seasons/regions (see Figure A1 in Appendix A), thus additional work can be done to improve MME prediction skill.

This research aims to facilitate a new approach module for MME prediction that uses relative dynamical diagnostic performance within the model instead of any external model forcing. In this study, we develop a climate filter [Lee et al., 2011] to evaluate individual constituent models based on the reproducibility of atmospheric responses to observed climate impacts, such as the El Niño-Southern Oscillation (ENSO) or North Atlantic Oscillation (NAO), with a focus on the East Asian summer monsoon (EASM) region during the boreal summer.

Previous researches point out that the EASM variations are intimately linked to the development and decay of El Niño or La Niña [e.g., Wang et al., 2008, 2009b]. Nevertheless, since the EASM has complex spatial and temporal structures that encompass the tropics, subtropics and mid-latitudes, its variability is influenced not only by the variations originated from the tropics (i.e., ENSO) [Chen and Chang, 1980; Huang and Lu, 1989; Ding, 2004; Ninomiya, 2004; Wu et al., 2006; Li et al., 2010], but also by those from the mid-latitudes to high latitudes [Enomoto et al., 2003; He et al., 2006; Ding and Wang, 2007; Wu et al., 2009, 2010]. Lee et al. [2005] also mentioned that the relationship between ENSO and summer rainfall over the northeast Asian region has not been clearly identified because the summer rainfall is significantly influenced by mid-latitude dynamics in addition to tropical circulation. Therefore, using a novel monsoon index, the authors separate the summer precipitation over the northeast Asian region into two precipitation components, being that associated with large-scale tropical circulation and that which is assumed to be associated with the dynamics of the mid-latitudes.

Wang et al. [2008] demonstrated the significant positive correlation between the PC1 of precipitation in JJA (0) and the Niño 3.4 SSTA in the previous winter D(-1)JF(0). Lee et al. [2005] showed a similar relationship between the lag-correlation

coefficients of the Niño SST and rainfall indices. Wu et al. [2009] used anomalous spring NAO to evaluate the relationship of the EASM with variances from the mid-latitudes and found the spring NAOI to be best correlated with the EASM. Gong et al. [2011] presented the relationship between the spring AO and summer monsoon indices and found that anomalies of summer precipitation and regional circulations are associated with the spring AO. Gong and Ho [2003] found a significant out of phase correlation between the late spring AO index and boreal summer rainfall along the Meiyu-Changma-Baiu rain belt on interannual time scales. The possible impact of North Atlantic SSTA of the preceding winter on EASM circulation has also been examined [Gu et al., 2009].

Building on the above, we have carefully considered several concerns related to the EASM. First, we consider which index is mainly suitable as an observed climate signal for the quantification of EASM variability. Second we evaluate what several attributes of the tropics and mid-latitudes most strongly influence the EASM. We also consider the relationship between the EASMI and influences associated with EASM, as well as determine the area of the EASM and the relationship between the EASMI and precipitation over the EASM region. We used four kinds of EASMIs and four kinds of EASM-related impacts respectively in this study.

The developed method based on the reproducibility of atmospheric responses to observed climate impacts over the EASM region is applied to hindcast seasonal prediction to demonstrate that limiting the constituent models of an MME to those with high fidelity will result in better prediction skill than is achievable by including all available models in an MME, as done in some operational centers. The ultimate goal is to show that MME prediction skills can be improved by limiting constituent models to those which clear a climate filter.

The rest of this paper is organized as follows. Section 2 describes the observed and individual models' data used, and defines the EASM indices investigated herein as well as the impacts associated with EASM variations. A climate filter concept is also introduced to grade the individual models. In section 3, the relative performances of the various MMEs are presented. Finally, a discussion of the results and study conclusion are presented in sections 4 and 5, respectively.

2. Data, EASM index and climate filter

2.1 Data used

In the present study, we use the National Centers for Environmental Prediction (NCEP)-Department of Energy (DOE) reanalysis 2 [Kanamitsu et al., 2002] and Climate Prediction Center Merged Analysis of Precipitation (CMAP) [Xie and Arkin, 1997] for the boreal summer seasons (June through August; henceforth JJA) for the period 1981-2003 as observations. In order to facilitate a new approach to MME prediction through evaluation of the relative performances and error of individual climate models, we adopt 10 operational seasonal prediction model hindcast outputs (see Table 1) for the same period that, in general, constitute a major portion of the operational MME of the APEC Climate Center (APCC), which is the most extensive operational MME setup employed today. Here we also adopt the APCC operational MME technique, known as the simple composite method [Peng et al., 2002; Kang et al., 2009; Lee et al., 2008, 2009, 2011]. In this technique, equal weights are assigned to the ensemble mean predictions of each of the models. Henceforth, MME means a simple composite method, unless otherwise specified.

Further, we follow the standard leave-one-out cross validation method [Michaelsen, 1987; Jolliffe and Stephenson, 2003; WMO, 2006; Kang et al., 2009] throughout the work. For example, we compute seasonal anomalies (of each model parameter as well as those from observations) from the corresponding climatological means that are obtained by excluding information from the target year for each year. The MME results are generated by combining the bias-corrected model forecast anomalies as a simple arithmetic mean of predictions based on individual models [Peng et al., 2002; Kang et al., 2009; Lee et al., 2008, 2009, 2011]. Then, hindcast performance can be verified by evaluating the unbiased performance of the component models.

Finally, we carry out a pilot forecast with the new MME approach for two boreal summer seasons, the JJA period of 2009 and 2010, to confirm the usefulness of the method.

Table 1 Description of the GCMs used

Member Economies	Acronym for Model	Organization	Model resolution
Australia	POAMA	Bureau of Meteorology Research Centre	T47L17
Canada	MSC_GEM	Meteorological Service of Canada	2°×2°L50
	MSC_GM2		T32L10
	MSC_GM3		T63L32
	MSC_SEF		T95L27
Chinese Taipei	CWB	Central Weather Bureau	T42L18
Korea	GCPS	Seoul National University	T63L21
	GDAPS_F	Korea Meteorological Administration	T106L21
	NIMR	National Institute of Meteorological Research	5°×4°L17
USA	NCEP	National Centers for Environmental Prediction	T62L64

2.2 EASM indices and impacts associated with EASM

First, we analyzed the statistical relationship between the East Asian summer monsoon and impacts from the tropics and mid-latitudes or high latitudes that influence the EASM. Four kinds of EASM indices and four kinds of EASM influence indices are investigated, including those of Wang and Fan [1999], Huang et al. [2004], Zhang et al. [2003], and Wang et al. [2001] for EASM, as well as the Niño 3.4 [Wang et al., 2008, among many others], NAO [Li and Wang, 2003], AO [Thompson and Wallace, 1998; Gong et al., 2011], and INA [Gu et al., 2009] indices for impacts associated with EASM. The indices are defined as follows.

A. East Asian summer monsoon Indices

- Wang and Fan (WF) index [Wang and Fan, 1999]: Lower-tropospheric vorticity anomalies
  - U850 averaged in (22.5-32.5°N, 110-140°E) minus U850 averaged in (5-15°N, 90-130°E)
  - This index was originally designed as a circulation index to quantify the variability of the WNP summer monsoon. The WF index reflects the variations in both the WNP monsoon trough and subtropical high, which are the key

elements of the EASM circulation system [Tao and Chen, 1987]. The WF index could potentially provide a useful measure of the subtropical and extratropical EASM. In this study, we used the reversed WF index (RWF).

- East Asia-Pacific (EAP) index [Huang et al., 2004]: Index measuring the interannual variation of the EASM
  - IEAP = − 0.25Z′s (60N, 125E)+0.50Z′s (40N, 125E)− 0.25Z′s(20N, 125E), where Z′s=Z′ sin 45/ sin φ is the standardized seasonal mean 500-hPa height anomaly at a grid point with the latitude φ , and Z′=Z−Z is the summer seasonal-mean 500-hPa height anomaly at the grid point.
  - Some previous studies show that the East Asian summer monsoon has a close relationship with the East Asia-Pacific (EAP) teleconnection pattern. Therefore, in this note based on the concept of the EAP teleconnection pattern, we define the EAP index as an index of the circulation anomalies of the East Asian summer monsoon.

- Zh index [Zhang et al., 2003]: Lower-tropospheric vorticity anomalies
  - U850 averaged in (10-20°N, 100-150°E) minus U850 averaged in (25-35°N, 100-150°E)
  - The EASMI was defined using the difference between the summer (JJA) mean anomalous wind of the above two regions at 850 hPa. There is a seesaw variation trend for the convective intensity between the tropical monsoon trough and Meiyu front over East Asia. We used the reversed Zhang index (RZh) in this study.

- YW index [Wang et al., 2001]: Meridional variation of the southerly component
  - V850 averaged in (20-30°N, 110-140°E) minus V850 averaged in (30-40°N, 110-140°E)
  - Difference between the summer (JJA) mean 850 hPa southerly anomalies averaged over the area EA II (the southern portion of the monsoon domain 20-30°N, 110-140°E) and over the area EA I (the northern part: 30-40°N, 110-140°E). The results indicate a delayed impact of El Niño on the EASM due to the significant correlation between the summer EASMI and the preceding autumn SST.

B. Impacts associated with East Asian summer monsoon

- Niño 3.4 index (DJF, previous winter) [Wang et al., 2008]: Variation of seasonal SSTA
  - SSTA averaged in (5°S-5°N, 170-120°W)
  - Wang et al., [2008] suggested that lead–lag correlation coefficients between the two PCs of rainfall and the Niño 3.4 SST anomaly from JJA(-) to JJA(+1) are calculated, and demonstrated significant positive correlation between PC1 of precipitation in JJA (0) and the Niño 3.4 SSTA in the previous winter D(-1)JF(0).

- North Atlantic Oscillation (NAO) index (AM, spring) [Li and Wang, 2003]: Variation of monthly sea level pressure
  - Difference in the normalized monthly sea level pressure (SLP) zonal averaged over the North Atlantic sector from 80°W to 30°E between 35°N and 65°N.
  - An anomalous spring NAO can induce a tripole SST pattern in the North Atlantic which sustains from spring through summer. The summer tripole SST anomalies contribute to the downstream development of subpolar teleconnections across northern Eurasia, which enhances (weakens) the high pressure over the Ural Mountain and the Okhotsk Sea. These anomalies favor a strengthened (weakened) East Asian subtropical front, namely, a strong (weak) EASM. Note that for comparison, the sign of the spring NAOI is reversed.

- Arctic Oscillation (AO) index (MAM, spring) [Thompson and Wallace, 1998, Gong et al., 2011]: Time coefficients of 1st EOF of monthly sea level pressure
  - Corresponding time coefficients of the first empirical orthogonal function (EOF) of the monthly sea level pressures (SLP) north of 20N
  - The spring AO index is the average for March, April and May. A high MAM AO will tend to enhance the horizontal wind shear at 850 hPa over East Asia in JJA, and will result in a significantly positive EASM index.

- North Atlantic SSTA (INA) index (DJF, previous winter) [Gu et al., 2009]: Variation of North Atlantic SSTA

- Difference of the normalized area-averaged SSTA between (40-55°N, 30-15°W) and (25-35°N, 75-60°W).
- An Index INA is defined to describe the variation of North Atlantic SSTA, which is closely related with mei-yu on the decadal timescale. Previous analyses indicate that the wintertime North Atlantic SSTA can have a delayed impact on East Asian circulation in the following summer.

Table 2 Temporal correlation between various EASMIs and indices related to the EASM. Superscripts a, b and c mean that the skill scores are significant at the 90%, 95% and 99% confidence levels, respectively, based on the two-tailed Student's t-test.

	EASMI (RWF, JJA)	Niño 3.4 (Prev. DJF)	NAOI (Rev. AM)	AOI (MAM)	INA (Prev. DJF)
EASMI (RWF, JJA)		0.61c	0.45b	0.39a	- 0.08
EASMI (EAP, JJA)	0.59c	0.55c	0.09	- 0.08	- 0.13
EASMI (RZh, JJA)	0.95c	0.70c	0.30	0.30	- 0.15
EASMI (YW, JJA)	0.73c	0.49b	0.13	0.32	0.15

C. Relationship between EASM indices and impacts associated with EASM

To confirm the relationships between the four kinds of summer monsoon indices we selected and the various EASM impact indices, we analyzed the temporal correlation coefficients between individual indices for the period of 1981-2003 (Table 2). Superscripts a, b and c mean that the correlation skill scores are significant at the 90%, 95% and 99% confidence levels, respectively, based on the two-tailed Student's *t*-test. The RWF index highly correlates with other EASM indices. The correlation coefficients are 0.59 for the EAP index, 0.95 for the RZh index, and 0.73 for the YW index, respectively. These similar correlations are all significant at the 99% level. It can be discerned that most of EASM indices are significantly correlated with the previous winter Niño 3.4 index. It is clear that the preceding winter Niño 3.4 is an important contributor to the interannual variability of the EASM. However, the preceding winter INA index shows the relatively poor relationship with the EASM

indices. We found that the spring (April-May, AM) NAO index and the spring (March-May, MAM) AO index are better correlated with the RWF index than are the other EASM indices. From these results, we decided to use the RWF index as the EASM index, and the preceding winter Niño 3.4 and spring NAO indices to capture impacts from the tropics and mid-latitudes.

2.3 Climate filter

Based on the abovementioned results, we perform a time series analysis of observed EASMI for summer (JJA) and NAOI for spring (AM) for the period of 1981-2003, and of the Niño 3.4 index for the previous winter (DJF) for the period of 1980-2002 (Figure 1). The RWF is employed as the EASMI. Figure 1 shows significant correlations between the indices, confirming the above results. The correlations of the observed indices with the EASMI are 0.61 (Niño 3.4 index) and 0.45 (NAOI) and are significant at the 99% and 95% confidence level, respectively, based on Student's two-tailed t-test. That is, the observed EASMI is very closely related to the observed ENSO and NAO forcing.

Figure 2 displays the observed temporal summer correlation pattern between precipitation and multiply regressed precipitation, on EASMI by EASMI, and original precipitation over the global (a) and East Asian (b) regions. From Figure 2a, it can be discerned that most significant positive correlation values are located within the western Pacific region including East Asia. The perfect correlation between precipitation and EASMI in the western Pacific region suggests that the East Asian summer monsoon region (Figure 2b) can be defined as the area from the equator to 60°N between 110°E and 160°E. We also calculated the pattern correlations as the relationship between the regressed observed precipitation, which is precipitation multiply regressed on EASMI by EASMI, and the original observed precipitation (Figure 3). The time average of the spatial pattern correlations is nearly 0.35. It is apparent that the year to year variations in correlation skill for summer precipitation over the EASM region are sensitive to the strength of the preceding winter ENSO, at least for the winters of 1982-1983 and 1997-1998, when the El Niño was strong.

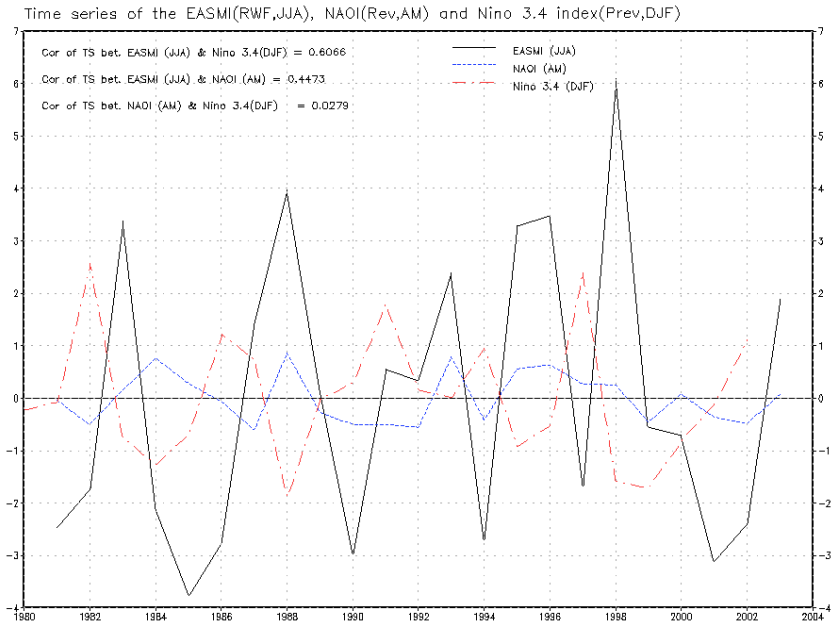

Figure 1 Time series of the EASMI, the spring (AM) NAO index for the period of 1981-2003 and the previous winter (DJF) Niño 3.4 index for the period of 1980-2002.

In Figure 4, we further try to compare the distribution of the EOF 1st mode pattern for the observed precipitation over the EASM region and regressed precipitation pattern on the EASM index. The rainfall distribution associated with the EASM shows a meridional tripole structure over East Asia and the western Pacific, which is characterized by enhanced precipitation over a tilted band-shaped region covering eastern China, Korea and the open ocean east of southern Japan, as well as by suppressed rainfall over the South China Sea and western Pacific including the Philippine Sea, Okhotsk Sea and areas between them. These similar structures are also shown in the first leading EOF patterns of precipitation. The time series of the corresponding principal component (PC) for the observed precipitation is given with the time series of the EASM index in Figure 4c, and their comparison shows the time evolution of the EASM index to be closely related to that of PC1. We have also computed the temporal correlation (0.86) between the PC time series and the EASM index and the spatial pattern correlation (0.85) between the first leading EOF pattern and the regressed precipitation pattern on the EASM index.

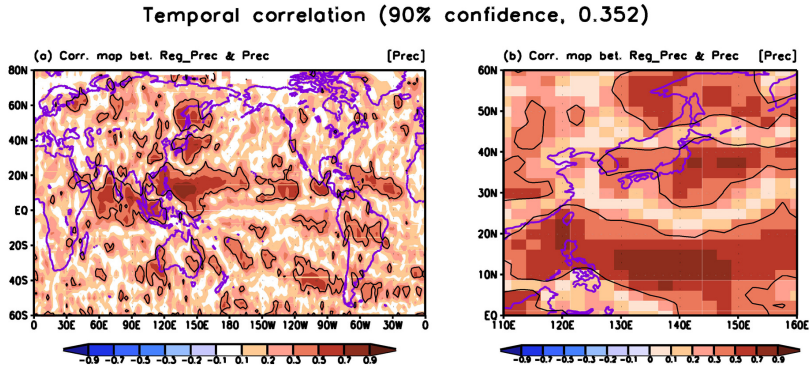

Figure 2 Observed temporal correlation pattern between the reconstructed rainfalls for each summer season over 23 years determined by applying the variability of the RWF index to the regressed rainfall pattern by projecting the observed global rainfall onto the corresponding RWF index and observed rainfall over the (a) global and (b) East Asian summer monsoon (110°E-160°E, 0°-60°N) regions. The contours represent a statistically significant positive correlation at a 90% confidence level.

Until now, we have examined the validity of the WF index as an EASM index, and that of the spring NAOI and previous winter Niño 3.4 index as impacts associated with EASM, as summarized in Table 2 and Figure 1. We have confirmed the relationship between the regressed rainfall on EASMI and original rainfall, as in Figure 2-4, shown the East Asia summer monsoon region to be 0-60°N, 110-160°E, and verified the relationship between rainfall and the EASM index. We use these concepts, in what we refer to as a climate filter, to grade the individual constituent models.

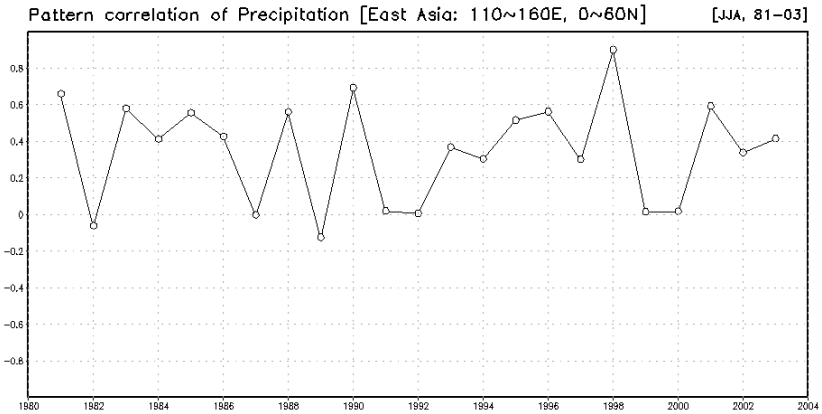

Figure 3 Time series of the spatial pattern correlations between the regressed observed precipitation, which is the multiply regressed precipitation pattern on EASMI, by EASMI, and the original observed precipitation.

On the basis of this verified relationships, we utilize the observed preceding winter Niño 3.4 index and the spring NAO index as weighting factors in the computation of the ENSO–associated EASMI and NAO-associated EASMI in the models. Then we apply the squared partial correlation coefficient (r^2, see Appendix B) between the zonal wind at 850 hPa (JJA) and the preceding winter Niño 3.4 (spring NAO) index adjusted for spring NAO (preceding winter Niño 3.4) index as the local weight for the EASMI and obtain the local ENSO (NAO)-associated EASMI. The magnitude of the squared correlation coefficient, known as coefficient of determination, is useful because it gives the proportion of the variance of one variable that is predictable from another variable, specifically as the ratio of the explained variation to the total variation. It is also one of the best means for evaluating the strength of the linear association between x and y. Thus, we believe that it is an appropriate means of representing the variance of EASMI associated with the previous winter Niño 3.4 index (spring NAO index).

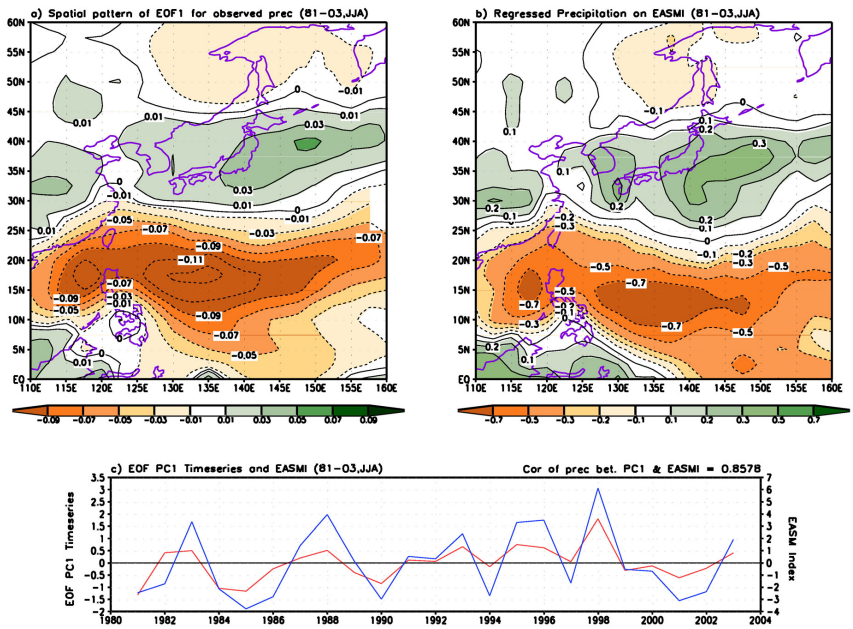

Figure 4 Distribution of (a) the EOF pattern for the observed rainfall and (b) regressed rainfall pattern on EASMI. (c) The corresponding principal component time series for observed rainfall (red line) and time series of EASMI (blue line) are shown. The temporal correlation between the PC time series of the observed rainfall and EASMI is given at the upper right.

Further, we carry out a scatter diagram analysis to identify the better performing models. For this, we first compute the ENSO (NAO)-associated EASMI defined by the U850 averaged in (90°~130°E, 5°~15°N) minus the U850 averaged in (110°~140°E, 22.5°~32.5°N) from the observed data for 23 boreal summers during the period 1981-2003. Similar ENSO (NAO)-associated EASM indices are also computed for each model based on its hindcasts. The observed ENSO (NAO)-associated EASM indices for each JJA season are plotted respectively against those from each model.

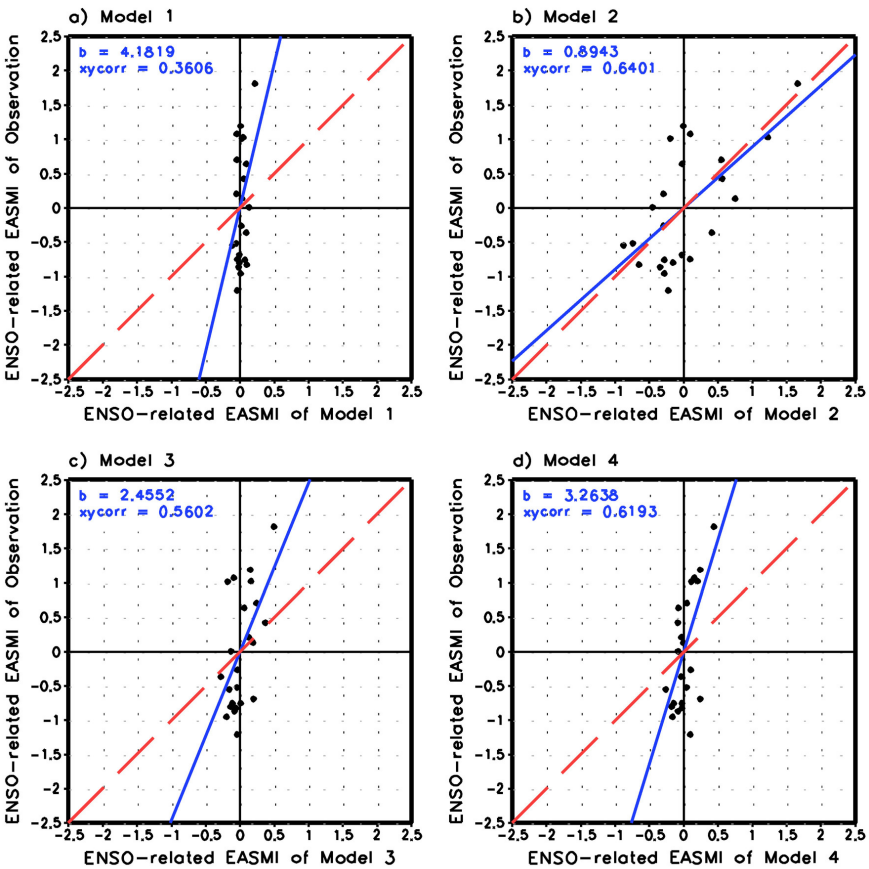

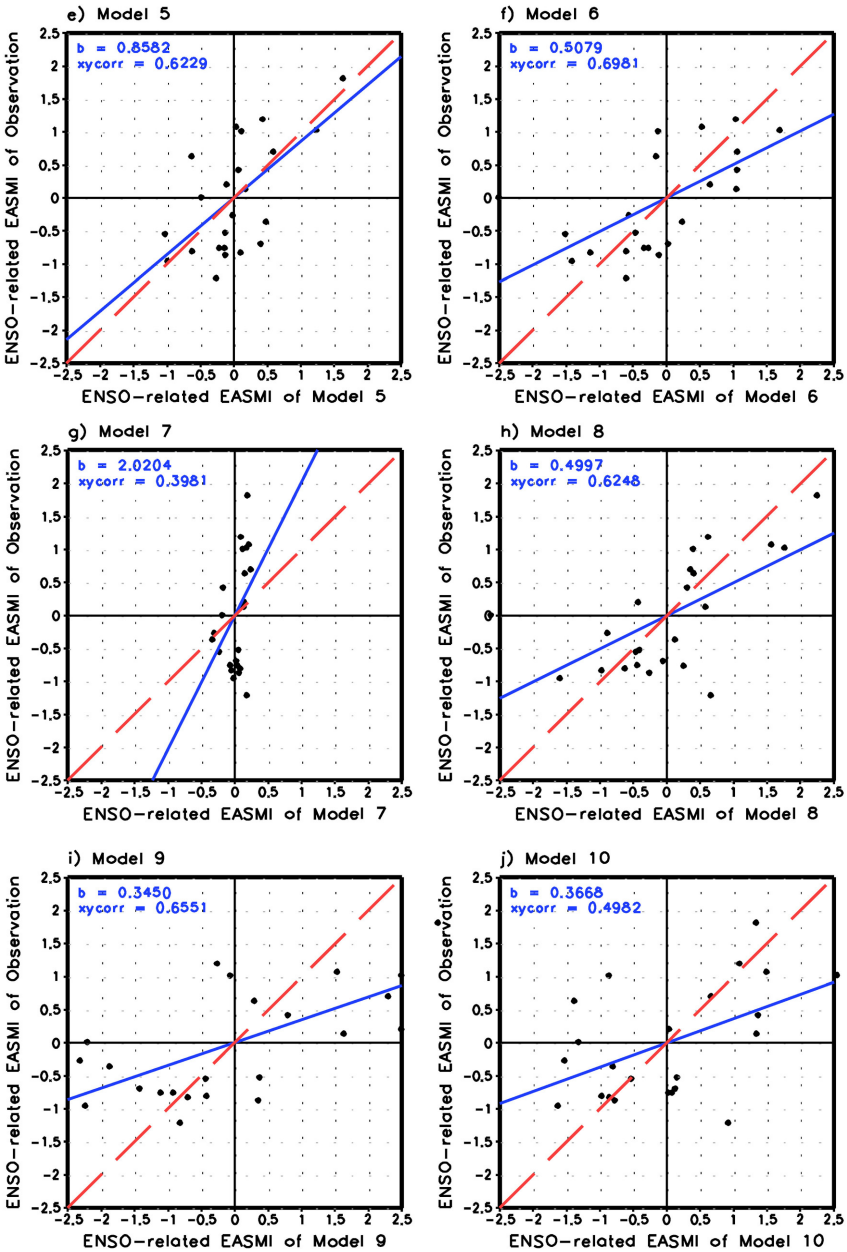

Figure 5 The ENSO-associated EASMI defined by the U850 in (90°~130°E, 5°~15°N) minus the U850 in (110°~140°E, 22.5°~32.5°N) from the observed data (Y-axis), for 23 boreal summers during the period 1981-2003, plotted against those from the individual models (X-axis). The blue solid line is the statistical line of fit, and the red dashed line is a reference diagonal line. The slope 'b' from the regression line of fit is provided in the upper left. The 'xycorr' stands for the temporal correlations between the observed data and model results.

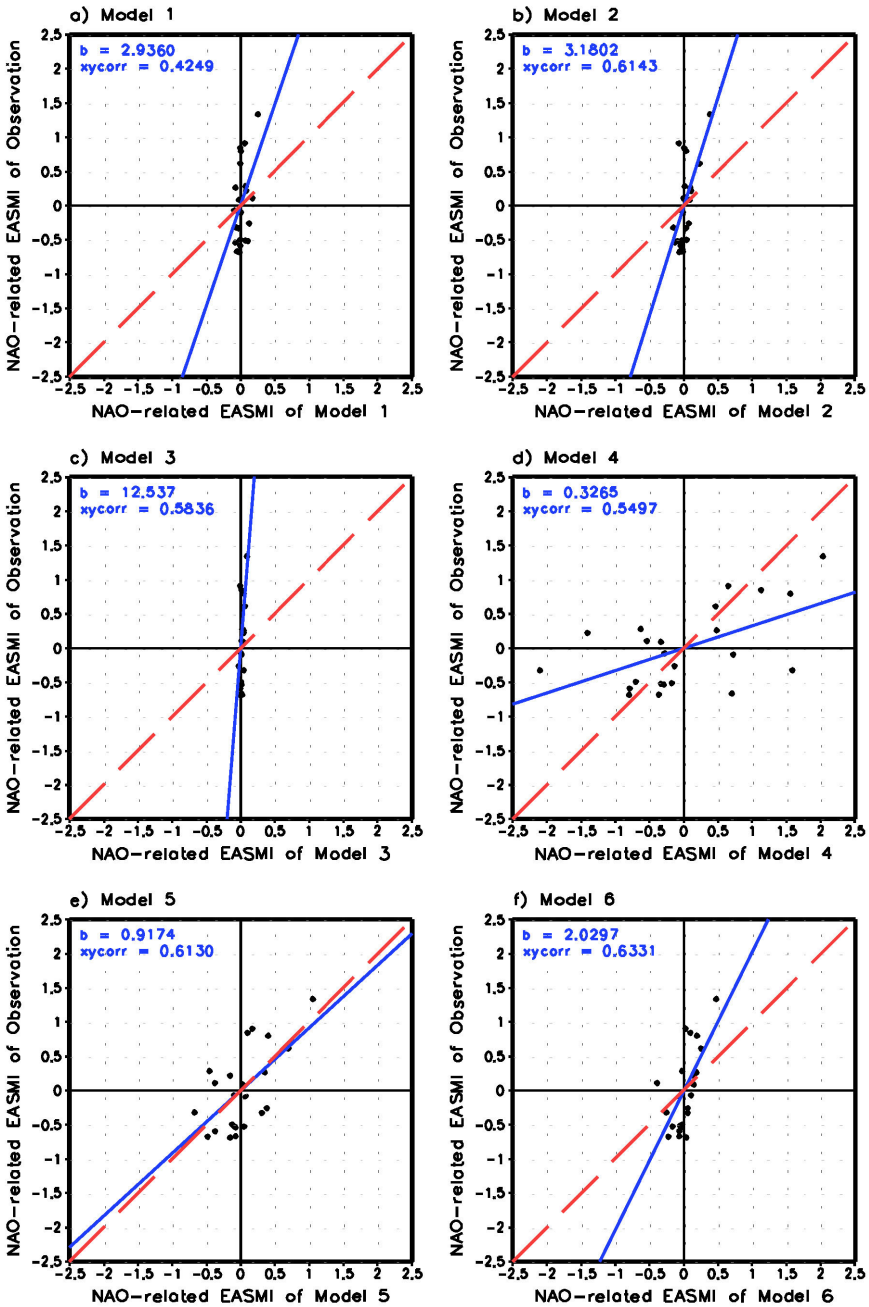
a) Model 1
b = 2.9360
xycorr = 0.4249
NAO-related EASMI of Observation
NAO-related EASMI of Model 1
b) Model 2
b = 3.1802
xycorr = 0.6143
NAO-related EASMI of Observation
NAO-related EASMI of Model 2
c) Model 3
b = 12.537
xycorr = 0.5836
NAO-related EASMI of Observation
NAO-related EASMI of Model 3
d) Model 4
b = 0.3265
xycorr = 0.5497
NAO-related EASMI of Observation
NAO-related EASMI of Model 4
e) Model 5
b = 0.9174
xycorr = 0.6130
NAO-related EASMI of Observation
NAO-related EASMI of Model 5
f) Model 6
b = 2.0297
xycorr = 0.6331
NAO-related EASMI of Observation
NAO-related EASMI of Model 6

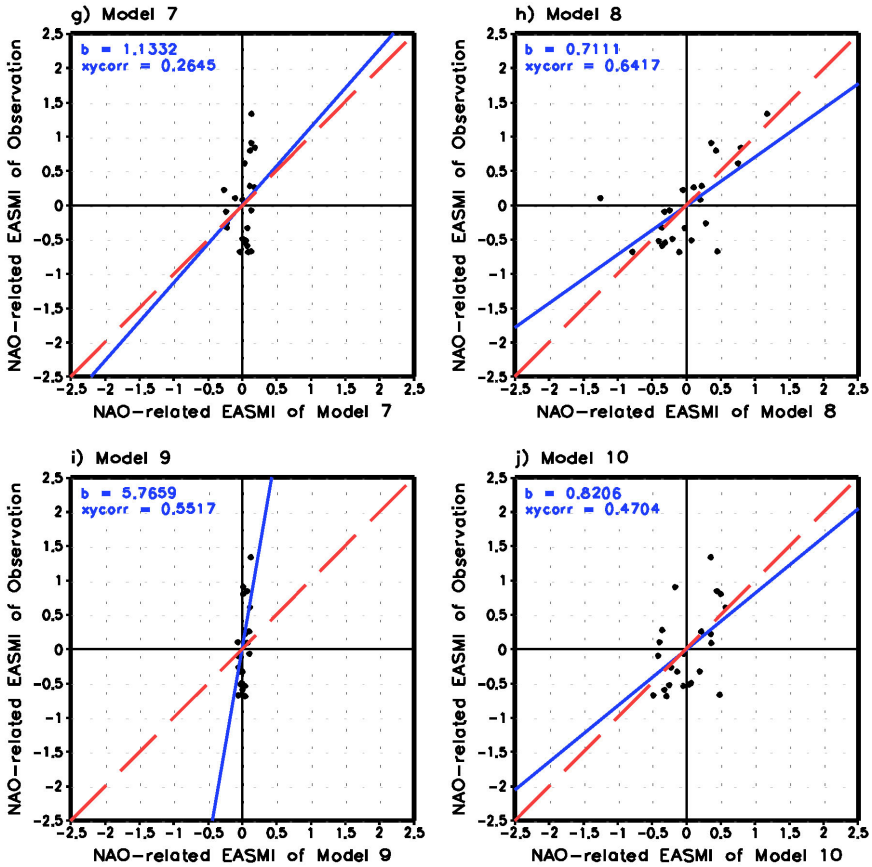

Figure 6 The same as in Figure 5 except for the NAO-associated EASMI.

The statistical significance of the correlations was computed based on the standard Student's two-tailed *t*-test [Spiegel and Stephens, 2008; Wilks, 1995; see also Appendix C]. The simple number of degrees of freedom for the temporal correlation over the 23-year span is 21. We further evaluate the statistical significance of the spatial pattern correlations by applying the effective spatial degree of freedom (ESDOF) [Snedecor and Cochran, 1980, Bretherton et al., 1999, Wang and Shen, 1999; see also Appendix D]. We follow the standard leave-one-out cross validation method [Michaelsen, 1987; Jolliffe and Stephenson, 2003; WMO, 2006; Kang et al., 2009] throughout the evaluation of hindcast skill. For example, we compute seasonal anomalies (of each model parameter as well as from observations) from the corresponding climatological means

that are obtained by excluding information from the target year, for each year, while carrying out the simple composite and climate filter methods. In case of the climate filter, the most skillful models are not the same for all hindcast periods because the sampling year differed for each target year, but we did find that the top 5 most skillful models consistently cleared the criteria for the entire study period of 1981-2003 (see Table E1 and E2 in Appendix E).

3. Evaluation of the hindcast relationship through the climate filter method

As mentioned earlier, we grade the models by evaluating the ENSO (NAO)-associated EASMI between the observed and model-simulated data. Scatter diagrams in Figures 5 and 6 depict the reproducibility of the relationships between the EASM indices and the Niño 3.4 and NAO indices, respectively, and identify those models which are more and less skillful. Note that two arbitrary conditions are used in the grading of each model as 'more skillful' or 'less skillful,' namely that (i) the slope of the fit between the observed and predicted EASM index should be larger than 0.5 and less than 1.5, and (ii) the temporal correlation coefficient between the observed and modeled data is greater than 0.4. Both criteria are based on the ~90% confidence level results of a Student's two-tailed *t*-test conducted for the study period. We found that only five out of the ten models satisfied the applied criteria. We refer to these 'more skillful' models, which successfully clear the climate filter at least for the boreal summer season, as class 'A' models, and the remainder are referred to as class 'B' models.

We examine three kinds of MME hindcast experiments over the study period. In the first experiment, henceforth referred to as 'A5', only the hindcasts from the class A models are used. In the second experiment, henceforth 'B5', only the class B models are used. In the third experiment, referred to as 'M10', the hindcasts from all 10 models are used. The spatial pattern correlations between the observed and predicted MME for precipitation and temperature at 850 hPa from all the three

experiments over the East Asian region are shown in Figures 7a and 7b. All three MME runs appear at first review to show similar interannual variation. However, the predicted skill performance varies significantly between the experiments (Table 3). Especially, it is noteworthy that the skill score of 0.34 (significant at the 85% confidence level from Student's two-tailed *t*-test; ESDOF=16.6) for rainfall in the A5 experiment is significantly higher than the corresponding skill score of 0.23 achieved by the B5 experiment (~ at the 70% confidence level from Student's two-tailed t-test; ESDOF=21.3), as shown in Figure 7a. The A5 skill score also exceeds that of the M10 experiment (0.32; significant at 85% confidence level from the two-tailed t-test; ESDOF=20.3). In order to further clarify the significance of the skillfulness of the three MME for precipitation prediction, we carry out an additional significance test by sorting the time averaged pattern correlations of five model combinations ($_{10}C_5$ = 252) from the given 10 models (see Figure F1 in Appendix F). After counting the number of combinations with prediction skills greater than those of each of the three MMEs, the ratios of the counted numbers to the number of possible calculations are calculated. The ratios are evaluated for significance and ordered, and from the ordering it is apparent that the A5 MME prediction skill (14/252, significant at 94.44% confidence level) is superior to the M10 MME skill (54/252, significant at 78.57% confidence level) and the B5 MME prediction skill (249/252, significant at 1.19% confidence level). Interestingly, the time averaged skills of the three MMEs, as used for predicting the 850 hPa temperature and shown in Table 3, are weaker than those of the same MMEs applied to precipitation, which needs further attention. It can be deduced that the prediction skill of the M10 MME is essentially attributable to the skill of the A5 MME.

Table 3 Time average of the spatial pattern correlations between the observed and various multi-model ensemble hindcast experiments (M10, A5 and B5) for precipitation and those for temperature at 850 hPa over the East Asian summer monsoon region. M10, A5, and B5 comprise 10 models and subsets of the same including the 5 most and 5 least skillful models, respectively.

Variables	Correlations		
	M10	A5	B5
Precipitation	0.323	0.343	0.226
850 hPa temperature	0.137	0.167	0.075

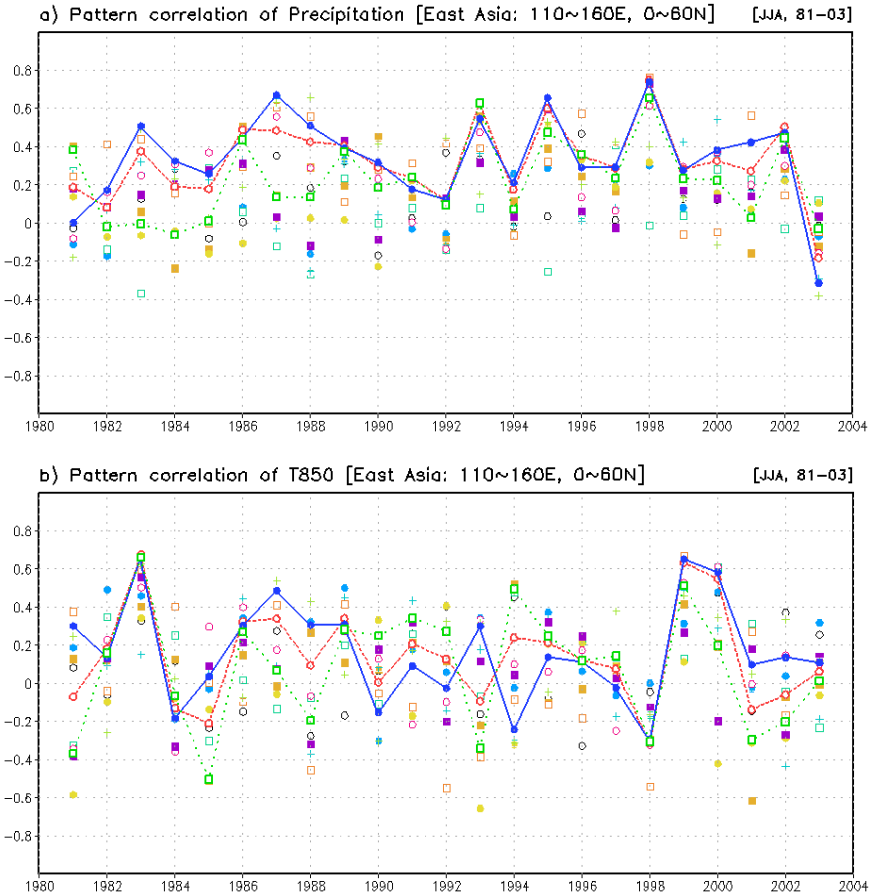

Figure 7 Time series of the spatial pattern correlations between the observed and the predicted (a) precipitation from M10 (dashed red line), A5 (solid blue line), B5 (dotted green line) and individual models (color marks) over the East Asian region. M10, A5 and B5 are the multi-model ensemble predictions based on a simple composite method using 10 models, and subset MMEs including the 5 more and 5 less skillful models, respectively. (b) Same as Figure 7a but for the 850 hPa temperature.

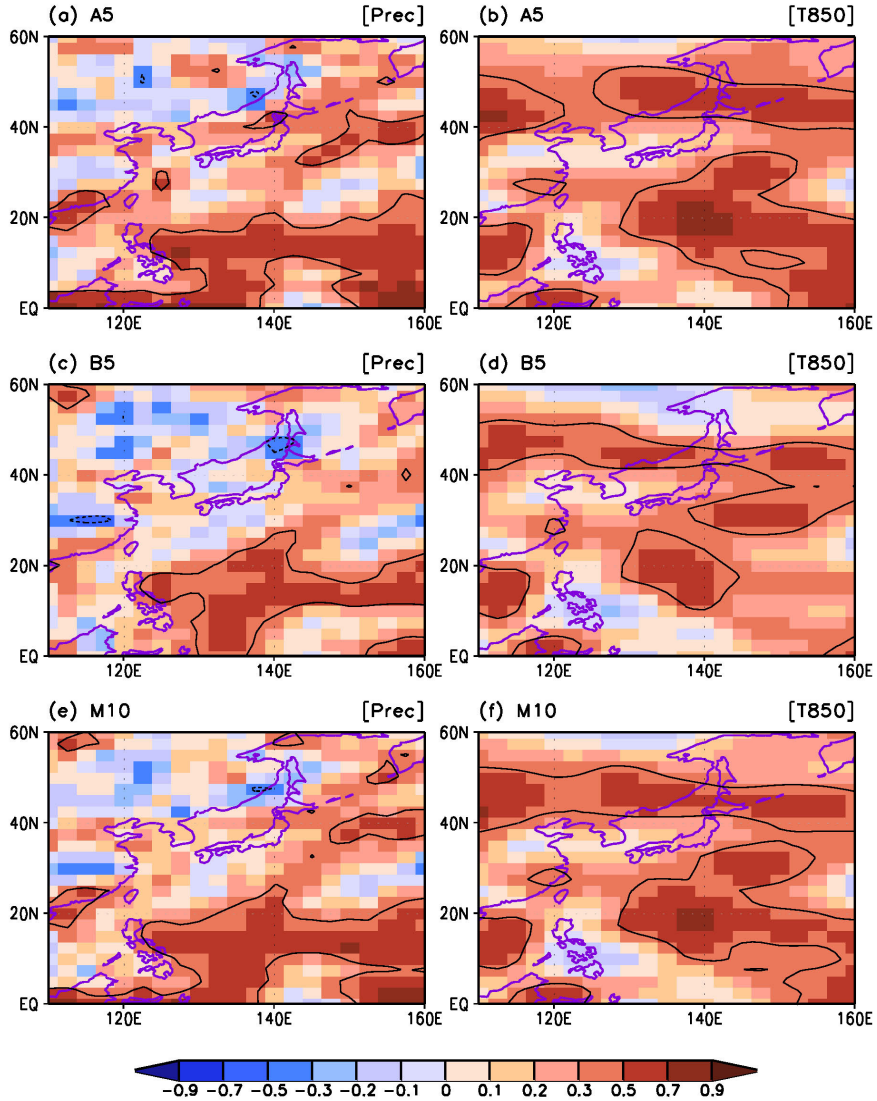

Figure 8 Temporal correlation coefficients between the observed and predicted precipitations (a, c, e), and those for the temperatures at 850 hPa (b, d, f) from the A5 (upper panels), B5 (middle panels) and M10 (lower panels) experiments. The contour lines represent statistical significance of the correlation coefficients at the 95% confidence level.

We also investigate the spatial distribution of prediction skills of all the MMEs for precipitation and temperature at 850 hPa by presenting, in Figure 8, the temporal correlation coefficient at each grid point for the period of 1981-2003. The statistical significance of the correlation coefficients was computed using Student's two-tailed *t*-test. The region of significant correlation at the 95% confidence level is outlined. High prediction skills for precipitation are generally confined south of 20°N, and those for 850 hPa temperature are higher north of 40-50°N in general and above 20°N over ocean areas. Though the prediction skills of the A5 MME are significantly superior to those of the B5 and M10 MMEs for both precipitation and temperature over the whole East Asian summer monsoon region, skill is shown to be lower over several regions including certain land areas north of 40°N, southern Japan and a few ocean areas.

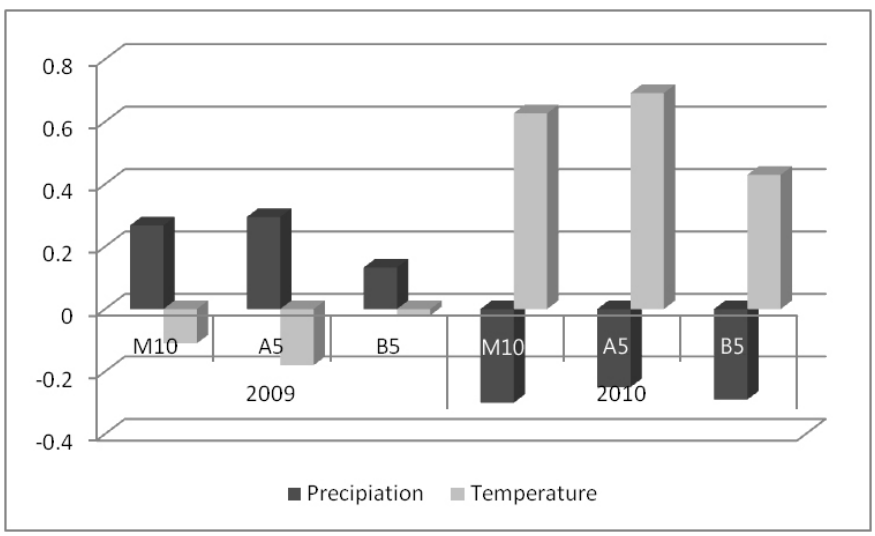

Figure 9 Spatial pattern correlations between the observed and the predicted precipitations (solid bars), and those for the temperature at 850 hPa (light-shaded bars) for two boreal summer seasons of June to August 2009 and June to August 2010 over the East Asia summer monsoon region (110°-160°E, 0°-60°N).

In order to explore the usefulness of the climate filter method for real-time seasonal prediction, we have applied the current method to MME prediction for the boreal summer seasons of June to August 2009 and June to August 2010 over the

East Asia summer monsoon region (110°-160°E, 0°-60°N). Figure 9 shows the spatial pattern correlations between the observed and predicted rainfall and temperature at 850 hPa over the East Asia summer monsoon region for the two summer seasons. In general, the precipitation and temperature prediction skills of the A5 MME are better than those of M10 and B5 MMEs. It is noted, however, that the skills of all three MMEs are particularly poor for 2009 temperature and 2010 precipitation for reasons that remain to be determined. Notwithstanding this disparity, the A5 MME is shown to generally give more skillful predictions than the M10 MME for the examined cases, and hence may be useful for real time seasonal prediction of precipitation and temperature.

4. Discussion

The method for grading the fidelity of model performance based on the strength of the association between the observed rainfall and local ENSO-associated Walker circulation in the tropical Pacific for the boreal winter seasons (DJF) of 1981-2003 has been discussed by Lee et al. [2011]. They showed that skillful models which clear the climate filter may accurately identify heat sources in the tropics, thus providing a better understanding of the teleconnection to the extra-tropics and beyond. The authors did not suggest the extensibility of their approach beyond their study scope. By employing the method, however, we found that it is difficult to grade the models as more skillful or less skillful based on the relationship between the ENSO-associated Walker circulation and tropical Pacific rainfall for the boreal summer season (JJA). Grading was found to be especially difficult for the East Asian monsoon region, due to the variability of EASM, which has complex spatial and temporal structures. Based on several previous works that evaluated the influence of the dynamics of the mid-latitudes and tropical circulation on the EASM [Wang et al., 2008, Lee et al., 2005; Wu et al., 2009; Gong et al., 2011; Gu et al., 2009], we have considered which climate signals are suitable to quantify the variability of the EASM and which impacts influence the EASM. We decided to use the RWF [Wang and Fan, 1999] index as the EASM index, and based on the relationship between the

EASM indices and impacts associated with the EASM, we selected the preceding winter Niño 3.4 [Wang et al., 2008] and the spring NAO indices [Li and Wang, 2003] to reflect impacts from the tropics and mid-latitudes. The developed method, which is based on the reproducibility of the ENSO- or NAO-associated EASMI as the climate signal over the EASM region, has been applied to retrospective and real forecasts to identify the better performing models among the constituent models. In fact, earlier researches employing several kinds of EASM indices have discovered that many observed climate impacts affect the EASM region, thus it may be useful to extend the scope of this investigation. Nonetheless, this research shows that the multi-model composite provides better skill if it employs constituent models that are generally more skillful. Though seasonal prediction by model simulation is still challenging for the EASM region, our research shows that realistic climate features can be well represented in MME seasonal prediction through the new approach.

5. Conclusion

We propose and demonstrate a new approach to MME prediction that enhances prediction skill using the relative dynamical diagnostic performance over the East Asian summer monsoon region during the period of 1981-2003. The NCEP-DOE reanalysis 2 [Kanamitsu et al., 2002], CMAP rainfall [Xie and Arkin, 1997] and APCC operational MME hindcast data sets are used in this study. Previous researches point out that the variability of the EASM, which has complex spatial and temporal structures, is influenced not only by variations originated from the tropics but also by those from the mid-latitudes. So, we investigated the statistical relationship between four kinds of indices [Wang and Fan, 1999; Huang et al., 2004; Zhang et al., 2003; Wang et al., 2001] for the EASM and four kinds of indices, namely the previous winter Niño 3.4 index [Wang et al., 2008], spring NAO index [Li and Wang, 2003], spring AO index [Gong et al., 2011] and the previous winter INA index [Gu et al., 2009], as impacts that influence the EASM from the tropics and mid-latitudes or high latitudes. We find that the observed RWF [Wang and Fan, 1999] index is relatively well related with the preceding winter Niño 3.4 and spring NAO indices of the observed data.

In addition, by evaluating the relationship between the observed regressed rainfall on EASMI and the observed real rainfall, we confirm the extent of the EASM region and show the RWF index to be an appropriate representation of the EASMI. Accordingly, we apply a climate filter that examines the degree of reproducibility of the above observed feature to grade model fidelity. We also explore the possible use of the above filter to devise an improved MME suite for seasonal prediction. It can be discerned that the prediction skill of our sample MME, involving all the available 10 models, is largely attributable to the five better models that successfully reproduce the EASMI. It is found that the gap between the skills of the MMEs comprising only the more skillful models, and only the less skillful models, significantly widens over the East Asian summer monsoon region. The study, however, is subject to the limitations of seasonal predictability and data length due to the complex spatial and temporal structure of the EASM region and the lack of a longer hindcast data set, respectively. Also, we understand that the effects of ENSO and the NAO are not the only main climate drivers that affect the East Asian summer monsoon. Nonetheless, our research shows that the novel model selection process enhances MME prediction skills such that realistic climate features can be well identified in both hindcast and forecast. Along with judicious use of climate filters such as that presented here, improved model characterization of physical and dynamical climate processes [Iizuka et al., 2003; Lee et al., 2008, etc], and use of data assimilation and initialization [Hudson et al., 2011, etc], will aid in the enhancement of MME seasonal prediction.

Appendix A

Hindcast Skill Scores of operational MME-based climate prediction at the APEC Climate Center (APCC)

The APCC produces dynamical seasonal prediction information through a state-of-the art multi-model ensemble prediction system that aggregates model predictions generated by APEC member economies every month. In turn, the APCC produces climate prediction information and performance statistics and disseminates these data to the APEC regions.

Figure A1 shows the prediction skills of the routine operational MME (colored bars) and individual models (grey bars) for precipitation and 850 hPa temperature for 23 boreal summers (JJA) during the period of 1981-2003. Four kinds of deterministic operational MME techniques are used. First, red bars indicate the simple arithmetic mean of the bias corrected predictions based on individual member models [*Peng et al*., 2002], the blue bars indicate the results of the pointwise multiple regression technique based on the training period [*Krishnamurti et al*., 2000], the black bars represent the results of the synthetic multi-model ensemble based on data which have been EOF-filtered to minimize residual error variance [Yun et al., 2005], the green bars reflect the results of the pointwise regression method for predicting the predictand at each grid point by projecting the predictor field onto the covariance pattern between the large-scale predictor field and the one-point predictand [*Kug et al*., 2008]. Finally, the yellow bars are the same as the red bars, except for the simple arithmetic mean carried out with the A5 MME, which comprised the five models that cleared the climate filter.

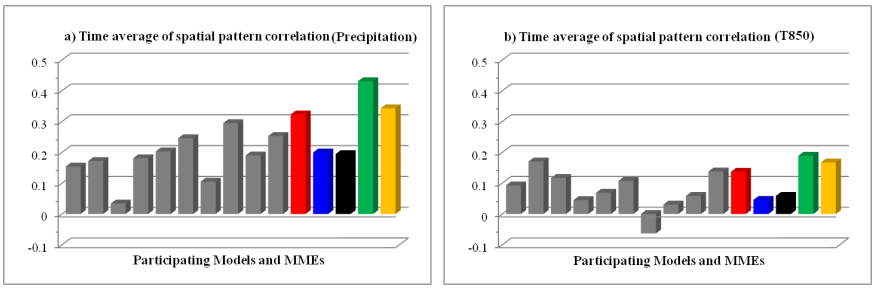

Figure A1 Time average of spatial pattern correlation coefficients between the observed and predicted precipitation for 23 boreal summers (JJA) during the period of 1981-2003 over the (a) East Asian (110°E-160°E, 0°N-60°N) regions. The grey bars are the hindcast skill scores of individual models involved in routine operational MME-based climate predictions at the APCC. The colored bars indicate the hindcast skills of the 4 operational deterministic multi-model ensemble methods employed by the APEC Climate Center; red (M10) and yellow (A5) bars are for the simple composite of bias corrected model ensemble means, the blue bars represent the multiple regression-based blend of model ensemble means, the black bars represent the synthetic multi-model ensemble based on multiple regression on the leading PCs of the EOF; the green bars present the stepwise pattern projection methods based on the pointwise regression method. Panels (b) is the same as Figure A1-(a), except for temperature at 850 hPa.

Appendix B

Partial correlation coefficients

It is often important to measure the correlation between a dependent variable and one particular independent variable when all other variables involved are kept constant; that is, when the effects of all other variables are removed.

The partial correlation coefficient $r_{12.3}$ between two variables A_1, A_2, after removing the influence of the variable A_3, is given by

$$r_{12,3} = \frac{r_{12} - r_{13}r_{23}}{\sqrt{(1 - r^2{}_{13})(1 - r^2{}_{23})}}$$

In abovementioned equation, the term r_{ij} represents the linear correlation coefficient between A_i and A_j. The partial coefficient $r_{12.34}$ between two variables A_1, A_2, after removing the influence of the variables A_3 and A_4, is obtained by

$$r_{12,34} = \frac{r_{12,4} - r_{13,4}r_{23,4}}{\sqrt{(1 - r^2_{13,4})(1 - r^2_{23,4})}} = \frac{r_{12,3} - r_{14,3}r_{24,3}}{\sqrt{(1 - r^2_{14,3})(1 - r^2_{24,3})}}$$

Further details are available from Wilks, 1995; Pedhazur, 1997; Spiegel, 2008, Ashok et al. 2007, etc.

Appendix C

Significance of correlation coefficient

We can think of a theoretical population coefficient of correlation, denoted by p, which is estimated by the sample correlation coefficient r. Tests of significance or hypotheses concerning various values of p require knowledge of the sampling distribution of r. Here, one tests the hypothesis that the correlation is zero (p=0).

$$t = \frac{r\sqrt{N-2}}{\sqrt{1-r^2}}$$

where we use the fact that this statistic has Student's distribution with $v = N-2$ degrees of freedom, N is the sample size. If the computed t value is as high as or higher than the percentile t value in table, then the researcher concludes the correlation is significant.

Appendix D

Method for Effective Spatial Degree of Freedom (ESDOF) estimation

The pattern correlation coefficients between two realizations of a field after the Fisher Z transformation are from a normally distributed population whose variance depends on the ESDOF [Wang and Shen, 1999] of the field. Namely, the variable

$$Z = \frac{1}{2}\ln\left(\frac{1 + r}{1 - r}\right)$$

is normally distributed, where r is the pattern correlation coefficient between two realizations of the field. The variance of the variable is

$$\mathrm{var}\,(\mathrm{Z}) = (\mathrm{esdof} - 3)^{-1}$$

$$\mathrm{esdof} = \frac{1}{\mathrm{var}(\mathrm{Z})} + 3$$

hence the ESDOF can be estimated if the variance of the Fisher Z transformed pattern correlation coefficient is known.

Appendix E

Model selection using the leave-one-out cross validation method

We have carried out the leave-one-out cross validation method [Michaelsen, 1987; Jolliffe and Stephenson, 2003; WMO, 2006; Kang et al., 2009] to grade the models on their skillfulness. The results can be seen in Tables E1 and E2. The models are separated based on the two criteria, which are that (i) the slope of the fit between the observed and predicted EASM indices should be more than 0.5 and less than 1.5, and (ii) the temporal correlation coefficient between the observed and modeled values is more than 0.4, the ~90% statistical confidence level for the study period (~ 20 years) based on Student's two-tailed *t*-test. Note that we rounded the numbers to the nearest hundredths. The tables indicate that five (models 2, 5, 6, 8 and 10; yellow cells) of the ten models satisfied the criteria.

Table E1 Model selection for ENSO weighting using the leave-one-out cross validation method (round off the numbers to the nearest hundredths)

Year	Participated Models									
1981	**Model1**	**Model2**	**Model3**	**Model4**	**Model5**	**Model6**	**Model7**	**Model8**	**Model9**	**Model10**
XYCorr	0.3402	0.6567	0.5482	0.6029	0.62	0.6997	0.384	0.6207	0.6479	0.5094
Slope	3.9272	0.9011	2.3848	3.2003	0.8419	0.501	1.9293	0.4897	0.3378	0.3682
1982	**Model1**	**Model2**	**Model3**	**Model4**	**Model5**	**Model6**	**Model7**	**Model8**	**Model9**	**Model10**
XYCorr	0.3441	0.6338	0.5568	0.6284	0.6221	0.695	0.4087	0.6211	0.6676	0.5058
Slope	4.0424	0.9125	2.4262	3.285	0.851	0.5034	2.0594	0.4944	0.349	0.3693
1983	**Model1**	**Model2**	**Model3**	**Model4**	**Model5**	**Model6**	**Model7**	**Model8**	**Model9**	**Model10**
XYCorr	0.3536	0.6041	0.5429	0.5935	0.5842	0.6715	0.3652	0.5883	0.6231	0.4382
Slope	3.9646	0.9027	2.3257	3.1059	0.8581	0.4957	1.8231	0.4858	0.3356	0.3538
1984	**Model1**	**Model2**	**Model3**	**Model4**	**Model5**	**Model6**	**Model7**	**Model8**	**Model9**	**Model10**
XYCorr	0.3537	0.6471	0.6147	0.7103	0.6624	0.7088	0.4027	0.6317	0.6431	0.5095
Slope	4.051	0.8904	2.7048	3.8517	0.907	0.5079	2.0127	0.4975	0.3401	0.3695
1985	**Model1**	**Model2**	**Model3**	**Model4**	**Model5**	**Model6**	**Model7**	**Model8**	**Model9**	**Model10**
XYCorr	0.3246	0.6462	0.5663	0.6874	0.6257	0.7005	0.4932	0.704	0.6561	0.5869
Slope	3.6476	0.863	2.3695	3.4676	0.8247	0.4886	2.4328	0.5406	0.331	0.4175
1986	**Model1**	**Model2**	**Model3**	**Model4**	**Model5**	**Model6**	**Model7**	**Model8**	**Model9**	**Model10**
XYCorr	0.4301	0.6216	0.5547	0.6209	0.6424	0.6839	0.3877	0.6082	0.6521	0.4807
Slope	5.0171	0.875	2.3892	3.207	0.866	0.4985	1.9344	0.486	0.3375	0.351
1987	**Model1**	**Model2**	**Model3**	**Model4**	**Model5**	**Model6**	**Model7**	**Model8**	**Model9**	**Model10**
XYCorr	0.3519	0.6345	0.5656	0.6459	0.6251	0.6938	0.442	0.6233	0.6511	0.4889
Slope	4.0854	0.8982	2.6839	3.4182	0.856	0.5113	2.3005	0.4962	0.3426	0.3698
1988	**Model1**	**Model2**	**Model3**	**Model4**	**Model5**	**Model6**	**Model7**	**Model8**	**Model9**	**Model10**
XYCorr	0.3919	0.6769	0.5458	0.5803	0.6142	0.6848	0.3907	0.6221	0.7014	0.4678
Slope	4.3261	0.8996	2.3024	3.0511	0.8136	0.4827	1.8938	0.4768	0.3516	0.3345
1989	**Model1**	**Model2**	**Model3**	**Model4**	**Model5**	**Model6**	**Model7**	**Model8**	**Model9**	**Model10**
XYCorr	0.3805	0.6506	0.5697	0.6254	0.6342	0.7951	0.4158	0.7493	0.6885	0.5166
Slope	4.6805	0.9225	2.5352	3.3242	0.8883	0.6563	2.1957	0.7151	0.3801	0.3932
1990	**Model1**	**Model2**	**Model3**	**Model4**	**Model5**	**Model6**	**Model7**	**Model8**	**Model9**	**Model10**
XYCorr	0.3416	0.6318	0.5518	0.609	0.6269	0.7101	0.4228	0.6286	0.6822	0.4822
Slope	3.9032	0.869	2.3757	3.1637	0.8441	0.5043	2.0976	0.4913	0.3509	0.3504
1991	**Model1**	**Model2**	**Model3**	**Model4**	**Model5**	**Model6**	**Model7**	**Model8**	**Model9**	**Model10**
XYCorr	0.3817	0.6519	0.5583	0.6254	0.6271	0.6974	0.3948	0.6337	0.676	0.4989
Slope	4.521	0.9154	2.4602	3.2983	0.8635	0.5102	2.0268	0.5081	0.3769	0.3667
1992	**Model1**	**Model2**	**Model3**	**Model4**	**Model5**	**Model6**	**Model7**	**Model8**	**Model9**	**Model10**
XYCorr	0.3607	0.6534	0.564	0.6221	0.6222	0.7041	0.3971	0.625	0.6631	0.505
Slope	4.1798	0.9452	2.5188	3.2793	0.8578	0.5214	2.0368	0.5028	0.3575	0.3836
1993	**Model1**	**Model2**	**Model3**	**Model4**	**Model5**	**Model6**	**Model7**	**Model8**	**Model9**	**Model10**
XYCorr	0.4078	0.6273	0.5402	0.6221	0.6085	0.6869	0.3676	0.6242	0.64	0.4878
Slope	4.7285	0.8771	2.4051	3.2264	0.8413	0.5009	1.9088	0.4919	0.3481	0.3556
1994	**Model1**	**Model2**	**Model3**	**Model4**	**Model5**	**Model6**	**Model7**	**Model8**	**Model9**	**Model10**
XYCorr	0.4005	0.6348	0.568	0.6189	0.6244	0.7017	0.4127	0.6462	0.6452	0.5077
Slope	4.6109	0.8758	2.4445	3.2098	0.846	0.502	2.0579	0.5079	0.3376	0.3669
1995	**Model1**	**Model2**	**Model3**	**Model4**	**Model5**	**Model6**	**Model7**	**Model8**	**Model9**	**Model10**
XYCorr	0.4429	0.6588	0.6264	0.6018	0.6468	0.7026	0.3553	0.5889	0.6363	0.4562
Slope	5.0338	0.8841	2.6586	3.098	0.8557	0.4931	1.7834	0.4767	0.3286	0.3356
1996	**Model1**	**Model2**	**Model3**	**Model4**	**Model5**	**Model6**	**Model7**	**Model8**	**Model9**	**Model10**
XYCorr	0.3696	0.6869	0.6592	0.6141	0.6369	0.7313	0.3816	0.6286	0.6823	0.5697
Slope	4.1361	0.9287	2.8613	3.1442	0.847	0.5136	1.8833	0.4864	0.3467	0.4104
1997	**Model1**	**Model2**	**Model3**	**Model4**	**Model5**	**Model6**	**Model7**	**Model8**	**Model9**	**Model10**
XYCorr	0.3368	0.6355	0.5491	0.6191	0.6217	0.6941	0.3774	0.6201	0.654	0.4912
Slope	4.1985	0.9289	2.4303	3.495	0.9129	0.5221	2.0084	0.4937	0.3418	0.3602
1998	**Model1**	**Model2**	**Model3**	**Model4**	**Model5**	**Model6**	**Model7**	**Model8**	**Model9**	**Model10**
XYCorr	0.1261	0.5101	0.4149	0.4866	0.4903	0.5975	0.3458	0.5225	0.5752	0.4459
Slope	1.5773	0.7774	1.8984	2.7401	0.7249	0.4577	1.5859	0.4148	0.2929	0.2993
1999	**Model1**	**Model2**	**Model3**	**Model4**	**Model5**	**Model6**	**Model7**	**Model8**	**Model9**	**Model10**
XYCorr	0.3929	0.6613	0.5655	0.6166	0.6485	0.7051	0.4047	0.6293	0.6567	0.4923
Slope	4.6616	0.929	2.6231	3.247	0.9019	0.5114	2.3125	0.5013	0.3564	0.3655
2000	**Model1**	**Model2**	**Model3**	**Model4**	**Model5**	**Model6**	**Model7**	**Model8**	**Model9**	**Model10**
XYCorr	0.3602	0.6383	0.5584	0.6319	0.6232	0.6966	0.4107	0.6251	0.6703	0.5025
Slope	4.1692	0.8956	2.4472	3.3452	0.857	0.5088	2.2989	0.5078	0.3712	0.3861
2001	**Model1**	**Model2**	**Model3**	**Model4**	**Model5**	**Model6**	**Model7**	**Model8**	**Model9**	**Model10**
XYCorr	0.3606	0.6366	0.5332	0.595	0.5923	0.6777	0.3957	0.5953	0.6293	0.459
Slope	4.0631	0.8683	2.337	3.1436	0.8481	0.4965	1.953	0.4897	0.3378	0.3452
2002	**Model1**	**Model2**	**Model3**	**Model4**	**Model5**	**Model6**	**Model7**	**Model8**	**Model9**	**Model10**
XYCorr	0.3512	0.642	0.5445	0.5992	0.6049	0.6934	0.4223	0.6161	0.6577	0.4786
Slope	4.0048	0.8801	2.373	3.2059	0.8382	0.4975	2.1042	0.4868	0.3398	0.3513
2003	**Model1**	**Model2**	**Model3**	**Model4**	**Model5**	**Model6**	**Model7**	**Model8**	**Model9**	**Model10**
XYCorr	0.3376	0.652	0.5605	0.6554	0.6888	0.7141	0.3812	0.6223	0.6587	0.5709
Slope	3.9491	0.8982	2.4249	3.4344	0.9612	0.5126	1.9335	0.4922	0.3422	0.4298
	Model1	**Model2**	**Model3**	**Model4**	**Model5**	**Model6**	**Model7**	**Model8**	**Model9**	**Model10**
No. of Selection	0/23	23/23	0/23	0/23	23/23	23/23	0/23	22/23	0/23	0/23

Table E2 Model selection for NAO weighting using the leave-one-out cross validation method (round off the numbers to the nearest hundredths)

Year					Participated Models					
1981	Model1	Model2	Model3	Model4	Model5	Model6	Model7	Model8	Model9	Model10
XYCorr	0.4209	0.6338	0.5706	0.5368	0.6103	0.6349	0.265	0.638	0.5432	0.4839
Slope	2.8682	3.2327	12.241	0.3177	0.9017	2.0057	1.1176	0.6988	5.6249	0.8309
1982	Model1	Model2	Model3	Model4	Model5	Model6	Model7	Model8	Model9	Model10
XYCorr	0.3954	0.5946	0.5813	0.5481	0.6153	0.6349	0.2753	0.6335	0.5763	0.4712
Slope	2.7748	3.1452	12.287	0.3201	0.9045	2.0003	1.1574	0.6949	5.921	0.8071
1983	Model1	Model2	Model3	Model4	Model5	Model6	Model7	Model8	Model9	Model10
XYCorr	0.4533	0.5856	0.5563	0.5442	0.5837	0.6086	0.264	0.6166	0.5178	0.4272
Slope	3.0544	3.236	12.081	0.3161	0.915	1.9772	1.1011	0.6977	5.5754	0.775
1984	Model1	Model2	Model3	Model4	Model5	Model6	Model7	Model8	Model9	Model10
XYCorr	0.4162	0.6217	0.6224	0.6323	0.644	0.6429	0.2773	0.6441	0.5432	0.489
Slope	2.8805	3.1982	13.539	0.3973	0.9695	2.0491	1.1844	0.709	5.7397	0.8522
1985	Model1	Model2	Model3	Model4	Model5	Model6	Model7	Model8	Model9	Model10
XYCorr	0.3982	0.6114	0.5843	0.6109	0.6204	0.6309	0.3213	0.7159	0.5429	0.5878
Slope	2.718	3.0862	12.213	0.3561	0.9019	1.9724	1.3567	0.7818	5.5439	1.0435
1986	Model1	Model2	Model3	Model4	Model5	Model6	Model7	Model8	Model9	Model10
XYCorr	0.4842	0.5984	0.5761	0.5462	0.6277	0.6175	0.2805	0.6297	0.5471	0.4526
Slope	3.3628	3.1143	12.234	0.3197	0.9227	1.9939	1.1822	0.6959	5.6369	0.7874
1987	Model1	Model2	Model3	Model4	Model5	Model6	Model7	Model8	Model9	Model10
XYCorr	0.4185	0.6109	0.5822	0.6097	0.626	0.6296	0.343	0.6467	0.5487	0.4645
Slope	2.9096	3.2003	12.841	0.38	0.9373	2.0344	1.6459	0.7143	5.7305	0.8268
1988	Model1	Model2	Model3	Model4	Model5	Model6	Model7	Model8	Model9	Model10
XYCorr	0.4548	0.6396	0.5561	0.4991	0.5887	0.6121	0.2324	0.6287	0.591	0.4165
Slope	2.9981	3.1577	11.677	0.3003	0.8602	1.912	0.9604	0.674	5.8937	0.7278
1989	Model1	Model2	Model3	Model4	Model5	Model6	Model7	Model8	Model9	Model10
XYCorr	0.4461	0.6185	0.5872	0.5598	0.639	0.7502	0.2786	0.7799	0.5961	0.501
Slope	3.3726	3.2047	12.617	0.3347	0.9793	2.7518	1.2153	1.0123	6.5556	0.9062
1990	Model1	Model2	Model3	Model4	Model5	Model6	Model7	Model8	Model9	Model10
XYCorr	0.4122	0.6011	0.595	0.5303	0.6114	0.6592	0.3008	0.6496	0.5903	0.4433
Slope	2.7775	3.0537	12.387	0.3102	0.8904	2.0482	1.2554	0.6985	5.9946	0.7647
1991	Model1	Model2	Model3	Model4	Model5	Model6	Model7	Model8	Model9	Model10
XYCorr	0.437	0.6149	0.5837	0.5496	0.6131	0.639	0.2723	0.6433	0.5926	0.4701
Slope	3.1497	3.1956	12.563	0.327	0.9192	2.0597	1.1841	0.717	6.5638	0.8203
1992	Model1	Model2	Model3	Model4	Model5	Model6	Model7	Model8	Model9	Model10
XYCorr	0.4322	0.6153	0.587	0.5548	0.6133	0.6352	0.2654	0.6411	0.5543	0.4738
Slope	3.0034	3.2137	12.817	0.3303	0.9171	2.0597	1.1365	0.7119	5.8857	0.8463
1993	Model1	Model2	Model3	Model4	Model5	Model6	Model7	Model8	Model9	Model10
XYCorr	0.4632	0.609	0.5791	0.5451	0.6077	0.6285	0.2481	0.6417	0.5493	0.4635
Slope	3.2725	3.1719	12.754	0.3237	0.9202	2.0447	1.0925	0.7079	5.9906	0.8112
1994	Model1	Model2	Model3	Model4	Model5	Model6	Model7	Model8	Model9	Model10
XYCorr	0.4564	0.6104	0.5765	0.5518	0.6122	0.63	0.2785	0.6573	0.5387	0.4809
Slope	3.1192	3.1188	12.247	0.3224	0.9025	1.993	1.1738	0.7161	5.6013	0.8244
1995	Model1	Model2	Model3	Model4	Model5	Model6	Model7	Model8	Model9	Model10
XYCorr	0.465	0.6574	0.6425	0.5135	0.6329	0.6378	0.1979	0.6014	0.528	0.4198
Slope	3.0516	3.2293	13.129	0.2984	0.8991	1.949	0.8338	0.6671	5.3307	0.723
1996	Model1	Model2	Model3	Model4	Model5	Model6	Model7	Model8	Model9	Model10
XYCorr	0.4189	0.722	0.729	0.5398	0.6243	0.6681	0.2213	0.6379	0.5856	0.5481
Slope	2.734	3.5613	15.162	0.3043	0.8813	2.0139	0.9053	0.6712	5.7537	0.9054
1997	Model1	Model2	Model3	Model4	Model5	Model6	Model7	Model8	Model9	Model10
XYCorr	0.4128	0.6132	0.578	0.5647	0.6207	0.635	0.2405	0.6358	0.5498	0.4643
Slope	2.8951	3.3224	12.419	0.3766	1.0003	2.1446	1.1053	0.7084	5.7167	0.8086
1998	Model1	Model2	Model3	Model4	Model5	Model6	Model7	Model8	Model9	Model10
XYCorr	0.1828	0.4313	0.4152	0.4224	0.4611	0.4975	0.2004	0.5303	0.438	0.4272
Slope	1.3611	2.6424	9.5011	0.2424	0.7267	1.6429	0.7568	0.5783	4.3498	0.6612
1999	Model1	Model2	Model3	Model4	Model5	Model6	Model7	Model8	Model9	Model10
XYCorr	0.4698	0.6293	0.5961	0.5492	0.6474	0.6407	0.2493	0.6582	0.5501	0.4636
Slope	3.3604	3.2606	13.796	0.325	0.9849	2.0479	1.1521	0.7305	5.9617	0.8158
2000	Model1	Model2	Model3	Model4	Model5	Model6	Model7	Model8	Model9	Model10
XYCorr	0.4244	0.6138	0.5834	0.5616	0.6142	0.6328	0.2762	0.644	0.5711	0.4816
Slope	2.9323	3.1826	12.528	0.3375	0.919	2.0338	1.297	0.7203	6.2826	0.8756
2001	Model1	Model2	Model3	Model4	Model5	Model6	Model7	Model8	Model9	Model10
XYCorr	0.4112	0.6195	0.556	0.5474	0.5851	0.6058	0.2529	0.6127	0.5153	0.4261
Slope	2.7741	3.1148	11.969	0.3164	0.8836	1.966	1.054	0.6976	5.5085	0.7619
2002	Model1	Model2	Model3	Model4	Model5	Model6	Model7	Model8	Model9	Model10
XYCorr	0.4207	0.6071	0.5674	0.5321	0.5942	0.6296	0.2874	0.6308	0.5559	0.4448
Slope	2.8465	3.0919	12.1	0.3138	0.8896	1.9814	1.2059	0.691	5.6802	0.7761
2003	Model1	Model2	Model3	Model4	Model5	Model6	Model7	Model8	Model9	Model10
XYCorr	0.4178	0.6186	0.5842	0.5744	0.6693	0.6443	0.253	0.6386	0.5492	0.5151
Slope	2.8876	3.1835	12.479	0.3426	1.0318	2.0567	1.0884	0.7059	5.7167	0.9204
	Model1	Model2	Model3	Model4	Model5	Model6	Model7	Model8	Model9	Model10
No. of Selection	0/23	0/23	0/23	0/23	23/23	0/23	0/23	23/23	0/23	23/23

Appendix F

Significance test for model combinations

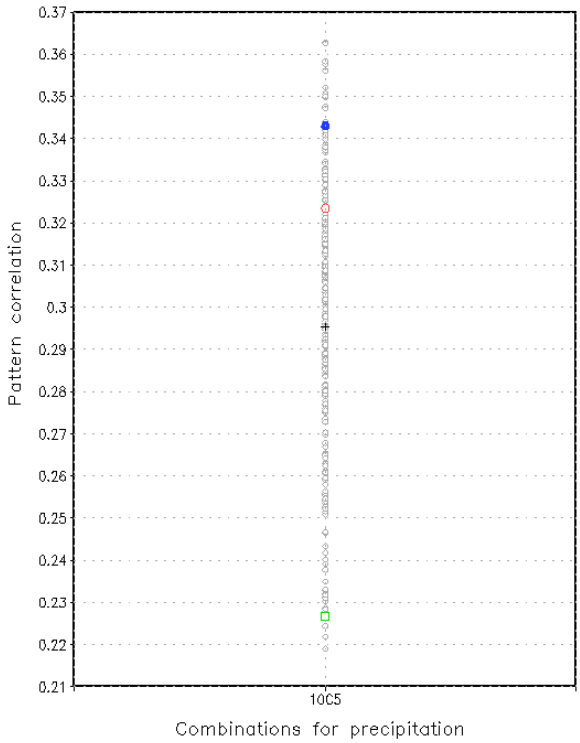

Figure F1 Time average of spatial pattern correlations between the observed and predicted precipitations over East Asia as computed by five combinations of 10 different models. There are 252 total combinations. The A5 (blue filled circle), M10 (red open circle) and B5 (green square) are multi-model ensemble predictions using 10 total models, as well as subsets of the 5 most and 5 least skillful models, respectively. The black cross mark indicates the average skill of the total combinations.

REFERENCES

Alves O, Wang G, Zhong A,Smith N, Tseitkin F, Warren G, Schiller A, Godfrey S, Meyers G, (2003), POAMA: Bureau of Meteorology operational coupled model seasonal forecast system. Proc. National Drought Forum, Brisbane, Apr 2003, pp. 49-56.

Ashok, K., H. Nakamura, and T. Yamagata (2007), Impacts of ENSO and IOD events on the Southern Hemisphere storm track activity during austral winter, J. Climate, 20, 3147-3163.

Barnston, A. G., S. J. Mason, L. Goddard, D. G. Dewitt, and S. E. Zebiak (2003), Multimodel ensembling in seasonal climate forecasting at IRI. *Bull. Amer. Meteor. Soc.* 84, 1783-1796.

Bretherton, C., M. Widmann, V. Dymnikov, J. Wallace, and I. Blade (1999), The effective number of spatial degrees of freedom of a time-varying field. *J. Climate*, 12, 1990–2009.

Chen, G. T. J., and C.-P. Chang (1980), Structure and vorticity budget of early summer monsoon trough (Mei-yu) over southeastern China and Japan, Mon. Weather Rev., 108, 942 – 953, doi:10.1175/1520-0493(1980)108←0942:TSAVBO→2.0.CO;2.

Ding, Y. H. (2004), Seasonal march of the east Asian summer monsoon, in East Asian Monsoon, edited by C.-P. Chang, pp. 3 – 53, World Sci., Singapore.

Ding, Q., and B. Wang (2007), Intraseasonal teleconnection between the summer Eurasian wave train and the Indian monsoon, J. Clim., 20, 3751– 3767, doi:10.1175/JCLI4221.1.

Doblas-Reyes, F. J., M. Deque, and J.-P. Piedelievre (2000), Multi-model spread and probabilistic seasonal forecasts in PROVOST. *Q. J. R. Meteorol. Soc.* 126, 2069–2088.

Doblas-Reyes, F. J., R. Hagedorn and T. N. Palmer (2005), The rationale behind the success of multi-model ensembles in seasonal forecasting – II. Calibration and combination. *Tellus* 57A, 234–252.

Enomoto, T., B. J. Hoskins, and Y. Matsuda (2003), The formation mechanism of the Bonin high in August, *Q. J. R. Meteorol. Soc.*, 129, 157– 178, doi:10.1256/qj.01.211.

Gong, D.-Y., and C.-H. Ho (2003), Arctic Oscillation signals in the East Asian summer monsoon, J. Geophys. Res., 108(D2), 4066, doi:10.1029/2002JD002193.

Gong, D.Y.; Yang J.; Kim S.J.; Gao Y.Q.; Guo D.; Zhou T.J. and Hu M. (2011), Spring Arctic Oscillation-East Asian summer monsoon connection through circulation changes over the western North Pacific. *Clim. Dyn.*, DOI 10.1007/s00382-011-1041-1

Gu, W., C. Y. Li, X. Wang, and W. Zhou, 2009: Linkage between mei-yu precipitation and North Atlantic SST on the decadal timescale. Adv. Atmos. Sci., 26(1), 101–108, doi: 10.1007/s00376-009-0101-5.

Hagedorn, R., F. J. Doblas-Reyes and T. N. Palmer (2005), The rationale behind the success of multi-model ensembles in seasonal forecasting – I. Basic concept. *Tellus* 57A, 219–233.

He, J. H., Z. W. Wu, Z. H. Jiang, C. S. Miao, and G. R. Han (2006), "Climate effect" of the northeast cold vortex and its influences on Meiyu, Chin. Sci. Bull., 51, 2803–2809.

Huang, R. H., and L. Lu (1989), Numerical simulation of the relationship between the anomaly of subtropical high over east Asia and the convective activities in the western tropical Pacific, Adv. Atmos. Sci., 6, 202–214, doi:10.1007/BF02658016.

Huang Gang (2004), An index measuring the interannual variation of the East Asian summer monsoon: The EAP index. Advances in Atmospheric Sciences, 21: 41-52.

Hudson, D., O. Alves, H. H. Hendon, and G. Wang (2010), The impact of atmospheric initialisation on seasonal prediction of tropical Pacific SST. *Clim. Dyn.* DOI 10.1007/s00382-010-0763-9

Iizuka, S., K. Orito, T. Matsuura and M. Chiba, (2003), Influence of cumulus convection schemes on the ENSO-like phenomena simulated in a CGCM, *J. Meteorol. Soc. Jpn.* 81, 805-827.

Jolliffe, I. T. and D. B. Stephenson (2003), *Forecast Verification: A Practitioner's Guide in Atmospheric Science*, John Wiley & Sons, Ltd, ISBN: 0-471-49759-2.

Kanamitsu, M., and co-authors (2002), NCEP-DOE AMIP-II Reanalysis (R-2), *Bull. Amer. Meteor. Soc.* 83, 1631-1643.

Kang, H., and co-authors (2009), Statistical Downscaling of Precipitation in Korea Using Multimodel Output Variables as Predictors, *Mon. Weather Rev.*, 137, 1928-1938

Krishnamurti, T. N., and co-authors (1999), Improved weather and seasonal climate forecasts from multimodel superensemble. *Science* 285, 1548-1550.

Krishnamurti, T. N., C. M. Kishtawal, D. W. Shin, C. E. Williford (2000), Multi-model superensemble forecasts for weather and seasonal climate. *J. Climate* 13, 4196-4216.

Kug, J.-S., J.-Y. Lee, and I.-S. Kang (2008), Systematic Error Correction of Dynamical Seasonal Prediction using a Stepwise Pattern Projection Method. *Mon. Weather Rev.*, 136, 3501-3512

Lee, E.-J., J.-G. Jhun, and C.-K. Park (2005), Remote connection of the northeast Asian summer rainfall variation revealed by a newly defined monsoon index. J. Climate, 18, 4381–4393.

Lee, D. Y., C.-Y. Tam, and C.-K. Park (2008), Effects of multicumulus convective ensemble on East Asian summer monsoon rainfall simulation, *J. Geophys. Res.*, 113, D24111, doi:10.1029/2008JD009847.

Lee, W.-J., and co-authors (2009), APEC Climate Center for Climate Information Services, *APCC 2009 Final Report* (Available at http://www.apcc21.net/activities/activities 03_01. php).

Lee, D. Y., K. Ashok, and J.-B. Ahn (2011), Toward enhancement of prediction skills of multimodel ensemble seasonal prediction: A climate filter concept, *J. Geophys. Res.*, 116, D06116, doi:10.1029 /2010JD014610.

Li JP and Wang J. (2003), A new North Atlantic Oscillation index and its variability. Advances in Atmospheric Sciences 20: 661–676.

Li JP, Wu ZW, Jiang ZH and He JH (2010), Can global warming strengthen the East Asian summer monsoon? *Journal of Climate*, DOI:10.1175/2010JCLI3434.1.

Michaelsen, J. (1987), Cross-validation in statistical climate forecast models, *J. Climate Appl. Meteor.*, 26, 1589-1600.

Min, Y.-M., V. N. Kryjov and C.-K. Park (2009), A Probabilistic Multimodel Ensemble Approach to Seasonal Prediction, *Wea. Forecasting*, 24, 812-828.

Ninomiya, K. (2004), Large- and mesoscale features of the Meiyu-baiu front associated with intense rainfalls, in East Asian Monsoon, edited by C.-P. Chang, pp. 404– 435, World Sci., Singapore.

Palmer, T. N., C. Brankovic, and D. S. Richardson (2000), A probability and decision-model analysis of PROBOST seasonal multi-model ensemble integrations. *Q. J. R. Meteorol. Soc.* 126, 2013-2034.

Palmer, T.N., A. Alessandri, U. Andersen, P. Cantelaube, and co-authors (2004), Development of a European multi-model ensemble system for seasonal to inter-annual prediction (DEMETER). *Bull. Amer. Meteor. Soc.*, 85, 853-872

Pedhazur, E. J. (1997), Multiple regression in behavioural research: explanation and prediction. Third edition U.S. A. Holt, Rinchart and Winston, Inc.

Peng, P., A. Kumar, H. van den Dool, and A. G. Barnston (2002), An analysis of multimodel ensemble predictions for seasonal climate anomalies, *J. Geophys. Res.* 107(D23), 4710.

Saha S, Nadiga S, Thiaw C, Wang J et al. (2006), The NCEP climate forecast system. J Climate 19: 3483-3517

Shukla, J., and co-authors (2000), Dynamical seasonal prediction. *Bull. Amer. Meteor. Soc.*, 81, 2493-2606.

Snedecor, G.W. and W.G. Cochran (1980), Statistical methods. Iowa State University Press, 7th ed., 507 pp.

Spiegel, M. R., L. J. Stephens (2008), Schaum's Outline of Theory and Problems of Statistics Fourth Edition, 577 pp., McGraw-Hill.

Tao, S., and L.-X. Chen (1987), A review of recent research on the east Asian summer monsoon in China, in Monsoon Meteorology, edited by C.-P. Chang and T. N. Krishnamurti, pp. 60– 92, Oxford Univ. Press, New York.

Thompson, D.W.J., and J.M. Wallace (1998), The Arctic Oscillation signature in the wintertime geopotential height and temperature fields. *Geophys. Res. Lett.*, 25, 1297-1300.

Wang, B., and Z. Fan (1999), Choice of South Asian Summer Monsoon Indices. Bull. Amer. Meteor. Sci., 80, 629-638.

Wang, Xiaochun, Samuel S. Shen (1999), Estimation of Spatial Degrees of Freedom of a Climate Field. *J. Climate*, 12, 1280-1291.

Wang, Y. F., B. Wang, and J.-H. Oh, 2001: Impacts of the preceding El Niño on the East Asian summer atmospheric circulation. *J. Meteor. Soc. Japan*, 79, 575–588.

Wang, B., Z. Wu, J. Li, J. Liu, C.-P. Chang, Y. Ding, and G. Wu (2008), How to measure the strength of the east Asian summer monsoon?, *J. Clim.*, 21, 4449– 4463, doi:10.1175/2008JCLI2183.1.

Wang, B., and co-authors (2009a), Advance and prospectus of seasonal prediction: assessment of the APCC/CliPAS 14-model ensemble retrospective seasonal prediction (1980–2004), *Clim. Dyn.* 33, 93–117.

Wang, B., J. Liu, J. Yang, T. Zhou, and Z. Wu (2009b), Distinct principal modes of early and late summer rainfall anomalies in east Asia, J. Clim., 22, 3864–3875, doi:10.1175/2009JCLI2850.1.

Wilks, D. S. (1995), Statistical Methods in the Atmospheric Sciences: An Introduction, 467 pp., Academic, San Diego, Calif.

WMO (2006), Standardised Verification System (SVS) for Long-Range Forecasts (LRF). New Attachment II-8 to the Manual on the GDPFS (WMO-No. 485), vol. I. 83 pp., Geneva, Switzerland.

Wu ZW, Li JP, He JH, Jiang ZH (2006), Occurrence of droughts and floods during the normal monsoons in the mid- and lower reaches of the Yangtze River. Geophysical Research Letters 33: L05813, DOI:10.1029/2005GL024487.

Wu ZW, Wang B, Li JP, Jin FF (2009), An empirical seasonal prediction model of the east Asian summer monsoon using ENSO and NAO. Journal of Geophysical Research 114: D18120, DOI:10.1029/2009JD011733.

Wu ZW, Li JP, Jiang ZH, He JH (2010), Predictable climate dynamics of abnormal East Asian winter

monsoon: once-in-a-century snowstorms in 2007/2008 winter. Climate Dynamics, DOI:10.1007/s00382-010-0938-4.

Xie, P., and P. A. Arkin (1997), Global precipitation: A 17-year monthly analysis based on gauge observations, satellite estimates, and numerical model outputs. *Bull. Amer. Meteorl. Soc.* 78, 2539-2588.

Yun, W.-T., and co-authors (2005), A multi-model superensemble algorithm for seasonal climate prediction using DEMETER forecasts. *Tellus*, 57A, 280-289.

Zhang, Q. Y., S. Y. Tao, and L. T. Chen, 2003: The interannual variability of East Asian summer monsoon indices and its association with the pattern of general circulation over East Asia (in Chinese). Acta Meteor. Sin., 61, 559–568.

APCC TECHNICAL REPORT 2011-02

- Improvement of MME Seasonal Prediction Skill
- Assessment of the Long-Lead Probabilistic Prediction
- Improvement of the APCC Probabilistic Multi-Model Ensemble Prediction

APEC Climate Center

12, Centum 7-ro, Haeundae-gu, Busan 612-020,
Republic of Korea
Tel: +82-51-745-3900 Fax: +82-51-745-3949
www.apcc21.org

비매품
94500
9 788997 533172
ISBN 978-89-97333-17-2
ISBN 978-89-97333-15-8 (세트)